Contents lists available at ScienceDirect

Applied Catalysis A, General

Check for updates

Nitrogen-doped graphdiyne for effective metal deposition and heterogeneous Suzuki-Miyaura coupling catalysis

Han Shen [a,b], Jingyi He [a,b], Feng He [a,b], Yurui Xue [a], Yongjun Li [a,b,*], Yuliang Li [a,b]

[a] *Beijing National Laboratory for Molecular Sciences (BNLMS), CAS Key Laboratory of Organic Solids, Institute of Chemistry, CAS Research/Education Center for Excellence in Molecular Sciences, Chinese Academy of Sciences, Beijing, 100190, PR China*
[b] *University of Chinese Academy of Sciences, Beijing, 100049, PR China*

ARTICLE INFO

ABSTRACT

For heterogeneous catalysts with nitrogen doped carbon materials as supporting substrates, accurate nitrogen (N) species and content is an important factor for promoting the catalytic activity. In this paper, N-doped graphdiyne (NGDY) was prepared from tetraethynylpyrazine (TEP) by bottom-up synthesis method as the support of metal nanoparticles. Specific pyridine nitrogen atoms are introduced in the N-doped carbon material. This unique structure makes it a promising material to support ultrafine metal particles or clusters. Microwave-assisted anchoring of Pd, Pt, Cu, Ni nanoparticles on NGDY generated novel hybrid composites, in which Pd-NGDY has high versatility for Suzuki-Miyaura reaction. DFT calculations revealed a charge transfer from NGDY to Pd NPs, and the free energy distribution showed a downward trend for Suzuki-Miyaura coupling reactions.

1. Introduction

Graphdiyne (GDY) [1], a novel material combining sp and sp^2 hybridized carbon in a conjugated structure, is attracting more attention of academic field as a member of carbon allotropes for its unique chemical and electron structure [2–5], and extraordinary performance in many fields, such as electrochemical catalysis [6,7] and batteries [8,9]. For further improving the electron distribution of carbon materials and adsorption capability of metal nanoparticles (NPs) toward reactants, nitrogen-doping is a common employed method. Reported nitrogen doped GDY (NGDY) has been used in electrochemistry [10–14] (however applications in other fields are relatively rare), in which the specific N atom has a significant impact on the performance of catalysis. Traditional pathway to prepare NGDY is the pyrolysis of nitrogen sources [11,12] that involve high thermal energy consumption and various N sites production. Considering the bottom-up synthesis of GDY, the synthesis of NGDY from suitable N-containing monomer is a unique and attractive way to obtain certain nitrogen species and content. Some works have been reported to prepare such NGDY [15,16], but little has been done in the preparation of NGDY with alternative hole topology, as well as the catalytic activity and charge transfer between NGDY and metal nanoparticles (NPs). Microwave irradiation is an effective

protocol for metal ion nucleation and NPs anchoring [17,18]. Metal NPs generate in diverse sizes and valence states under different irradiation conditions [17,19]. In addition, microwave irradiation is a facile way to help the formation of holes in 2D substrates (such as graphene) for anchoring metal catalysts [20–23]. Graphene-based supports with vacancy defect sites also play important roles in enhancing charge transfer between metal catalysts and supports to promote catalysis performance [24–28]. Therefore, it is economical and convenient to deposit NPs on our NGDY with natural pore structure by microwave deposition.

Large π conjugated network makes GDY a promising substrate for anchoring metal NPs to prepare composite heterogeneous catalysts [29, 30], so does NGDY. In comparison, homogeneous catalysts usually show super high efficiency because of its good molecular dispersion, but this advantage also brings difficulties to the separation and recovery of catalysts [31]. As for heterogeneous catalysts, although their efficiency is relatively low, they have attracted extensive attention due to the advantages of recovery and recycling [32,33]. Heterogeneous catalysts with metal NPs immobilized on the surface of supporting materials are commonly used in various organic reactions [34]. Good supporting materials can effectively prevent the aggregation of active metal NPs and improve the activity of the catalysts [31]. Therefore, it is an important issue to choose proper supporting materials. A large number

---

* Corresponding author at: Beijing National Laboratory for Molecular Sciences (BNLMS), CAS Key Laboratory of Organic Solids, Institute of Chemistry, CAS Research/Education Center for Excellence in Molecular Sciences, Chinese Academy of Sciences, Beijing, 100190, PR China.
E-mail address: liyj@iccas.ac.cn (Y. Li).

of materials have been used as supporting materials, such as polymer [32], MOFs [35], graphene [21,36], graphene derivate [20,37], etc. In this paper, sp²-N-graphdiyne (NGDY) was successfully applied as the substrate for loading different metal nanoparticles (Pd, Pt, Cu and Ni), and a variety of hybrid materials were prepared (Fig. 1). In addition, the typical Suzuki-Miyaura reaction was used as a model reaction to investigate the effect of substrate on the performance of NPs based heterogeneous catalyst. Pd-NGDY was introduced into Suzuki-Miyaura reaction as a highly active catalyst, and NGDY served as a stabilizer for metal nanoparticles as well as electron reservoir through donor-acceptor charge transfer. The natural pore structure, the N atoms and diyne groups in the substrate will benefit the binding of metal nanoparticles and enhance the charge transfer ability. The prepared Pd-NGDY complex showed high heterogeneous catalytic activity (TOF number of 1287 h^{-1} for iodobenzene) in Suzuki-Miyaura reaction, which was higher than commercial Pd-C counterpart and the pristine GDY based heterogeneous catalysts.

2. Experimental section

2.1. Materials

Most of the chemical reagents were analytically pure and purchased commercially from local supplier, and used directly without further handling unless otherwise stated. All reactions are performed under argon stream.

2.2. Instruments for preparation and characterization

NPs deposition was carried out in a Biotage initiator microwave machine with temperature and reaction time as the dominating setting parameters. SEM images were taken with a Hitachi Model S-4800 field emission scanning electron microscope. The NGDY film on Cu plates was directly used for SEM observation. TEM and HRTEM images accompanied by EDS were captured with a JEM-2100 F transmission electron

microscope with an accelerating voltage 200 kV. The TEM sample was prepared by dispersing NGDY films or Pd-NGDY powders in ethanol and transferred on the surface of Cu grids. Raman spectra were recorded with a Renishaw-2000 Raman spectrometer of resolution of 2 cm^{-1} by using of the 514.5 nm line of an Argon ion laser as the excitation source. X-ray photoelectron spectroscopy (XPS) was conducted with the Thermo Scientific ESCA Lab 250Xi using 200 W monochromat Al Kα radiation. X-ray powder diffraction pattern (XRD) were performed with a Japan Rikagu D/max-2500 rotation anode X-ray diffractometer equipped with graphite-monochromatized Cu Al Kα radiation in a 2θ range from 10 to 80° at a speed of 2° per minute at room temperature. NMR spectra were recorded with a Bruker AVANCE III (400 MHz) spectrometer. The GC–MS samples were analyzed by Agilent 5977B. The acquired EXAFS data were processed according to the standard procedures using the ATHENA module implemented in the IFEFFIT software packages. The k3-weighted EXAFS spectra were obtained by subtracting the post-edge background from the overall absorption and then normalizing with respect to the edge-jump step. Subsequently, k3-weighted χ(k) data of Ru K-edge were Fourier transformed to real (R) space using a hanning windows (dk = 1.0 Å^{-1}) to separate the EXAFS contributions from different coordination shells. To obtain the quantitative structural parameters around central atoms, least-squares curve parameter fitting was performed using the ARTEMIS module of IFEFFIT software packages.

2.3. DFT calculations

All density functional theory (DFT) calculations were performed with Vienna ab-initio simulation package (VASP) in order to investigate the periodic structures [38,39]. Geometry optimization of all the intermediates involved in reactions was carried out with the Perdew-Burke-Ernzerbof (PBE) form of generalized gradient approximation functional (GGA) for exchange correlation functional [40]. During the configuration optimization and energy calculations, the plane wave cutoffs energy of 400 eV and the 3 × 3×1 Monkhorst – Pack
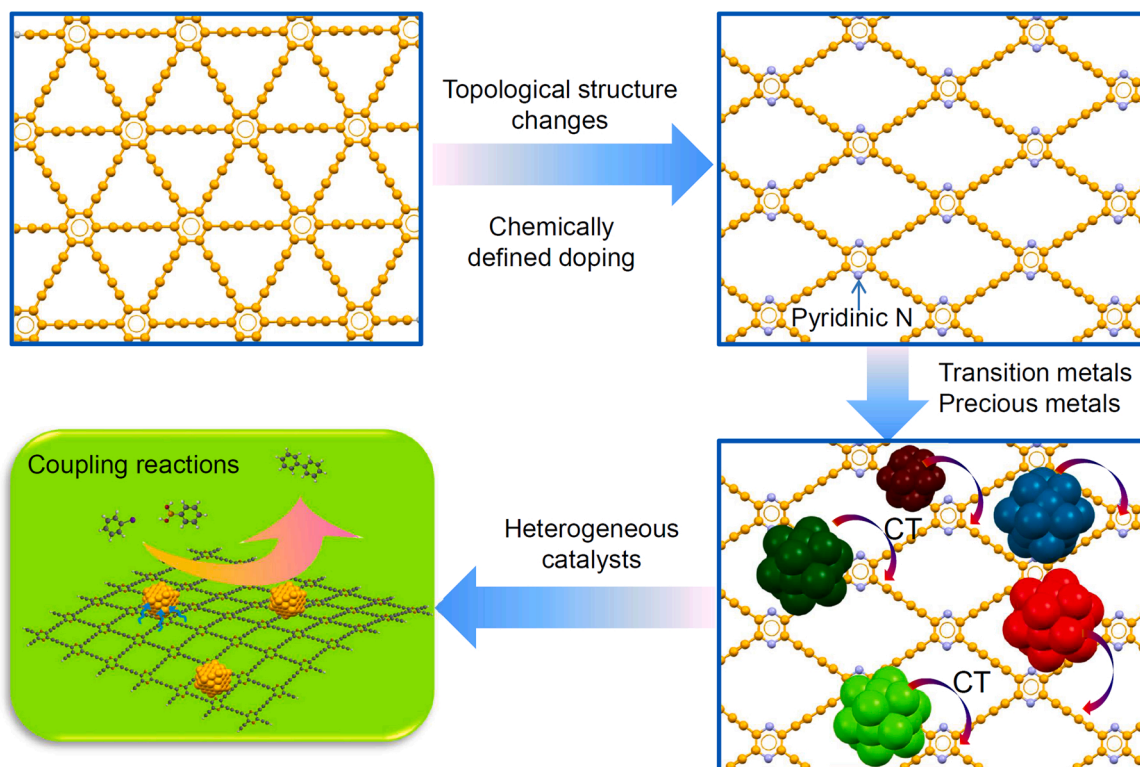

Fig. 1. Design principle for the N-doped graphdiyne applied for the support of metal nanoparticles.

k-points grids were set, respectively [41]. To describe the vdw interaction, the dispersion corrections DFT-D3 was employed. Besides, the spin polarization was considered throughout the calculations. According to the method developed by Nørskov et al., the Gibbs free energy change (ΔG_{ads}) of H atom involved in reactions is obtained by using the free energy of $1/2H_2$ (g) [42]. To construct the model of Pd nanocluster supported on N doped GDY for catalyzing the Suzuki reaction, a 2×2 supercell of NGDY and a four atoms nanocluster of Pd were chosen.

2.4. Synthesis

2.4.1. Synthesis of precursors

Precursors were synthesized according to the reported routes [1,43]. As shown in Scheme 1, tetrachloropyrazine was synthesized through chlorination of 2,5-dioxopiperazine by phosphorus pentachloride in phosphorus oxychloride at 60 °C. Tetra[(trimethylsilyl)ethynyl] pyrazine (TEP-TMS) was synthesized through Negishi reaction where tetrachloropyrazine reacted with [(triethylsilyl)ethynyl] zinc chloride catalyzed by Pd(PPh₃)₄ in newly distilled THF under 80 °C for 2 days. Crude products were purified through column chromatography and characterized through mass spectrum (MS) and nuclear magnetic resonance spectrum (NMR).

2.4.2. Synthesis of NGDY

Tetra-butyl ammonium fluoride (TBAF, 1 M, THF solution) was used to get rid of the protecting groups to obtain monomer. Monomer was dissolved in methanol and added dropwise into the reaction mixture containing pyridine and copper plates under argon protection. The mixture was heated to 50 °C for 2 days. The NGDY film was exfoliated from Cu plates in $(NH_4)_2S_2O_8$ aqueous solution and cleaned by deionized water and ethanol. After drying under vacuum at 45 °C overnight, the product was obtained as dark brown films and grounded into powder for use.

2.4.3. Fabrication of nano hybrids

We took microwave irradiated deposition method to fabricate Pd-, Pt-, Cu-, Ni-NGDY and Pd-GDY. Take the Pd-NGDY as an example. Firstly, 70 mg as-prepared NGDY powder was dispersed into 60 mL ethylene glycol through strong ultrasonication. Then, 10 mg (0.034 mmol) Na₂PdCl₄ dissolved in 4 mL ethylene glycol was added into the quasi-homogeneous colloid with vigorous stirring. The mixture was stored in several 2−5 ml quartz tubes and saturated with Ar. The reduction reaction was carried out in a microwave organic synthesis equipment with the temperature and time parameters set as 160 °C, 2

min. The resulting product was collected by centrifugation and cleaned by ethanol and deionized water repeatedly. At last, it was dried under vacuum overnight. Other nano hybrids were prepared using the same method except for transition metal NPs that hydrazine hydrate was involved as the reductant. H₂PtCl₆·6H₂O, CuSO₄·5H₂O, NiCl₂·6H₂O were the precursor chemicals for Pt-, Cu-, Ni-NGDY, respectively. Specifically, the mixture of NGDY and H₂PtCl₆·6H₂O in ethylene glycol was neutralized by addition of NaOAc before used in the microwave deposition.

2.5. Catalytic tests

The general procedure for catalyzing the Suzuki- Miyaura reactions is described as follow. 0.5 mmol aryl halides, 0.75 mmol phenylboronic, and 1 mmol K₂CO₃ were dissolved in 10 ml solvent with continuous stirring. 10 mg catalyst was added into the mixture and the temperature was raised to required temperature. The progress was monitored and the conversion and yields (20 μL periodically) were analyzed by GC–MS. Less volatile compounds were purified through column chromatography and characterized by ¹H NMR and ¹³C NMR. Recycled Pd-NGDY was collected through centrifugation and cleaned thoroughly by water and ethanol, and dried for next cycle.

3. Results and discussion

3.1. Synthesis and structural characterizations

The nitrogen atoms in the basic pyrazine unit provide a large number of lone pair electrons, which can coordinate with metal atoms, showing the potential application prospects as support materials. Scheme 1 illustrates the bottom-up synthesis of NGDY. In general, the synthesis route of NGDY is similar to that of graphdiyne [7]. After removing the protecting group, the monomer was dissolved in methanol, dropped into the mixture of pyridine and copper plate, and NGDY was grown in situ on copper surface. NGDY was exfoliated from the copper plate and cleaned thoroughly with HCl (aq), deionized water, and ethanol. Anchoring of metal nanoparticles (Pd, Pt, Ni, and Cu) was conducted in a microwave reactor with a mixture of NGDY and metal salts (detailed information see Experimental Section). Metal ions grew into nanoparticles under microwave irradiation. The accurate mass loadings were determined by inductively coupled plasma mass spectrometry (ICP-MS) to be 1.07 %, 20.51 %, 1.91 %, 9.12 %, and 1.9 % for Pd-, Pt-, Cu-, Ni-NGDY and Pd-GDY, respectively.

The typical SEM and TEM images with different magnifications were
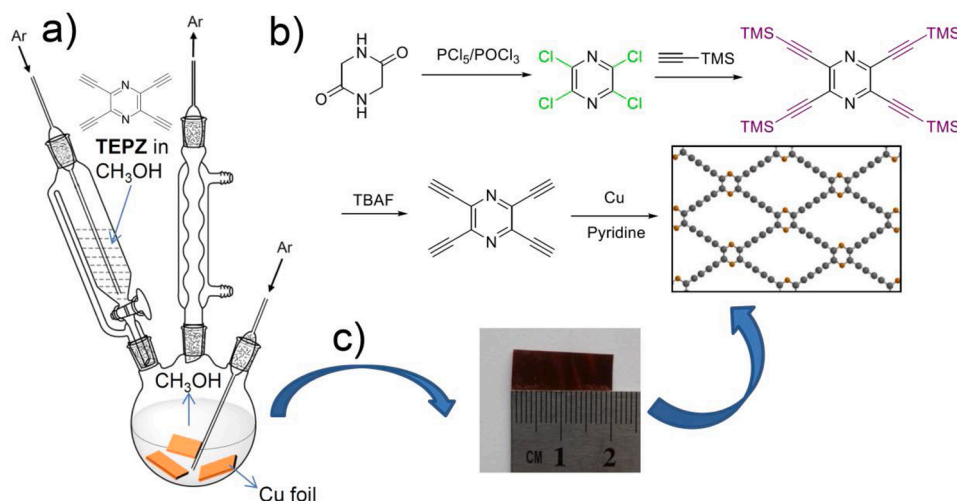
Scheme 1. Illustrations of the synthesis of NGDY through bottom-up pathway: a) experimental apparatus; b) synthetic route; c) the photo of NGDY growing on Cu plate.

shown in Fig. 2, from which the morphology and microstructure of the pristine NGDY, Pd-, Pt-, Cu-, Ni-NGDY can be easily observed. It can be seen that the pristine NGDY is a large-area smooth, transparent and flexible film (Fig. 2a–c).

In addition to the amorphous morphology, some fringe pattern with average distance of 0.36 nm was observed, which was consistent with that of the carbon (002) surface. After the metal deposition, TEM images of the nano hydrides revealed a large number of grain-like ultrafine metal nanoparticles (NPs) anchored on the surface of NGDY (Fig. 2d, g, j,

and m). The statistical measurement of NPs distribution (Fig. 2e, h, k, and n) showed that the average size of transition metal NPs was larger than that of noble metal NPs due to the addition of reductant in the process of transition metal nucleation. HRTEM images (Fig. 2f, i, l, o) clearly showed lattice fringes of 0.223 nm and 0.192 nm corresponding to Pd (111) and (200), 0.228 nm and 0.197 nm to Pt (111) and (200), 0.279 nm and 0.236 nm to Cu (110) and (111), and 0.201 nm to Ni (111). The TEM images of Pd-GDY were shown in Fig. S1. The average diameter of Pd NPs on GDY was larger than that on NGDY, and the
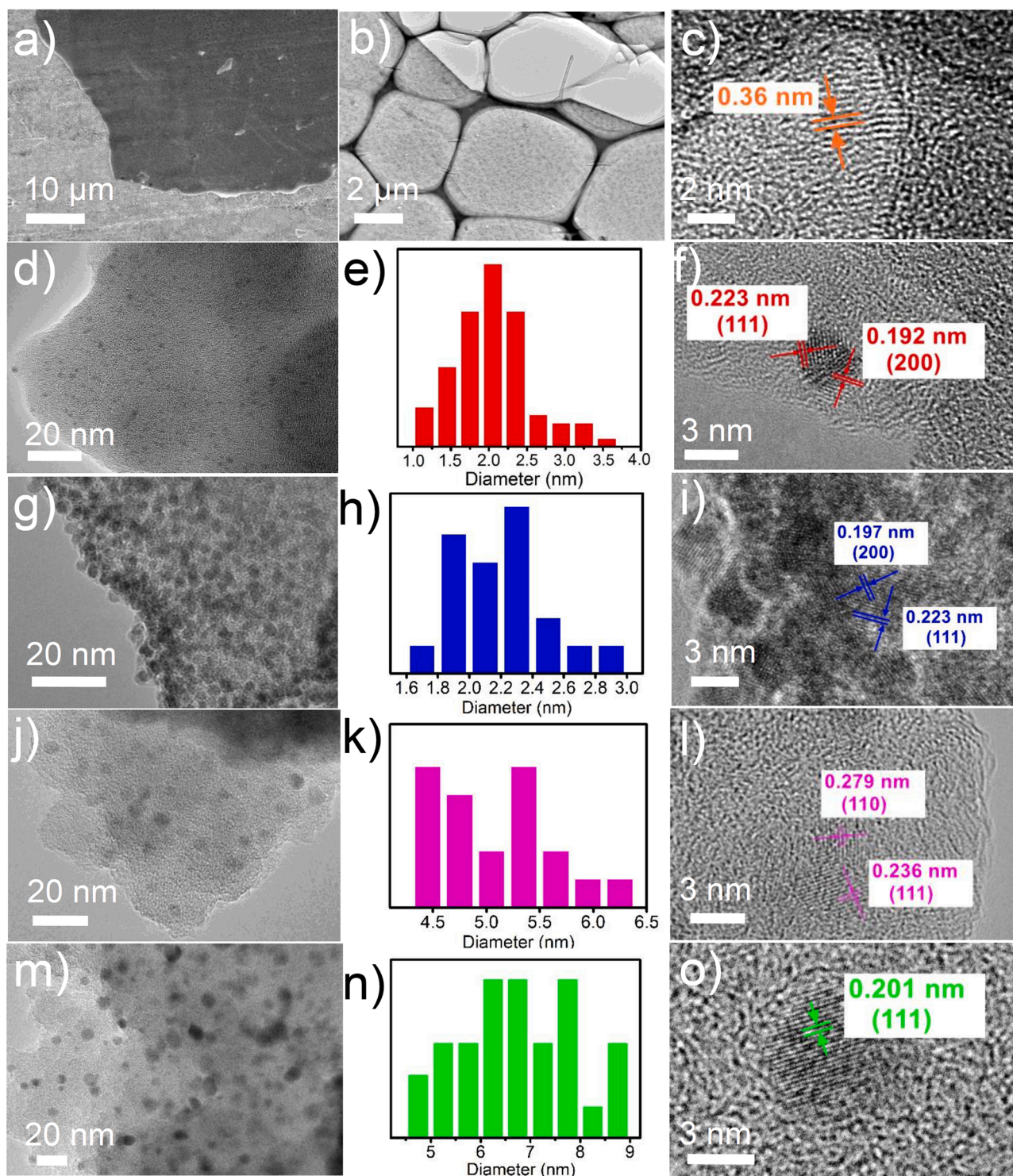

Fig. 2. a) SEM, b) TEM, c) HRTEM images of NGDY. TEM images of d) Pd-, g) Pt-, j) Cu-, m) Ni-NGDY. Size distribution of e) Pd-, h) Pt-, k) Cu-, n) Ni-NGDY. HRTEM images of f) Pd-, i) Pt-, l) Cu-, o) Ni-NGDY.

dispersion uniformity was poor, which showed that N-doping was beneficial to the dispersion and stability of NPs.

In order to understand the chemical composition and valence states of NGDY-hybrids, X-ray photoelectron spectroscopy (XPS) measurements were carried out and the spectra were shown in Fig. 3a–f. The representative XPS survey scan spectrum (Fig. S2) reveals the existence of C, N and O elements in pristine NGDY. Fig. 3a–d showed the high-resolution (HR) XPS spectra of Pd 3d, Pt 3d, Cu 2p and Ni 2p on NGDY, respectively, all of which have zero metal valence and oxidized valence. The binding energy values of the metal NPs were recorded and listed in Table S1. Based on area ratio, the metallic Pd(0) content in Pd-NGDY (81 %) was higher than that in Pd-GDY (75 %), implying that N centers might stabilize better zero valent metals [44]. Compared with the data reported in literature [45,46], the binding energy values of Pd 3d of Pd NPs on NGDY and GDY both shifted obviously toward lower energy region (Fig. 3a and Table S1), indicating the strong electron donating effect of both support materials. In addition, the binding energy value of $Pd°3d_{5/2}$ of Pd-NGDY is even lower than that of Pd-GDY, while $Pd^{II}3d_{5/2}$ of Pd-NGDY is higher than that of Pd-GDY, which is also an evidence for the above hypothesis. The same happens for Pt-NGDY and Pt-GDY (Fig. 3b and Table S1) [29,47,48]. As for other transition metals, although the ratio of zero/oxidized states are influenced by introduction of reducing agent, a higher content of zero valent state was observed in NGDY hybrids. Compared with Ni 2p of Ni NPs on

GDY, Ni 2p of Ni NPs on NGDY showed similar shift toward lower binding energy (Fig. 3d) [49]. Exceptionally, opposite shift of Cu 2p of Cu NPs on NGDY was observed as compared with that on GDY (Fig. 3e) [50]. All the XPS results indicate that NGDY might be an excellent stabilizer for zero valent metals and showed strong charge transfer with metal NPs.

In addition, taking the Pd-NGDY as an example, the changes of C and N XPS signals before and after metal NPs loading were studied to investigate the influence of N doping and the interaction between metal NPs and the substrate. Compared with GDY, C=N peaks (Fig. S3) were observed in NGDY except for typical C 1s peaks. The high-resolution C 1s peaks of NGDY and Pd-NGDY were compared in Fig. 3e, in which ignorable change of five main peaks of C1s after loading Pd-NPs was observed. For N 1s HR-XPS (Fig. 3f), there are three peaks corresponding to protonated pyrrolic-N (400.1 eV), pyrazine-N (399.2 eV), and pyridinic-N (398.4 eV) on pyrazine ring [44]. Protonated pyrrolic-N and pyrazine-N (area ratio 1:1) might come from complexation of pyrazine-N with impure molecules. After loading Pd NPs, the proportion of protonated pyrrolic-N and pyridinic-N increased simultaneously, which also indicated that N atoms were involved in metal coordination. There results indicated that N atoms played important roles in modifying the surface electron density and promoting the nucleation of metal ions.

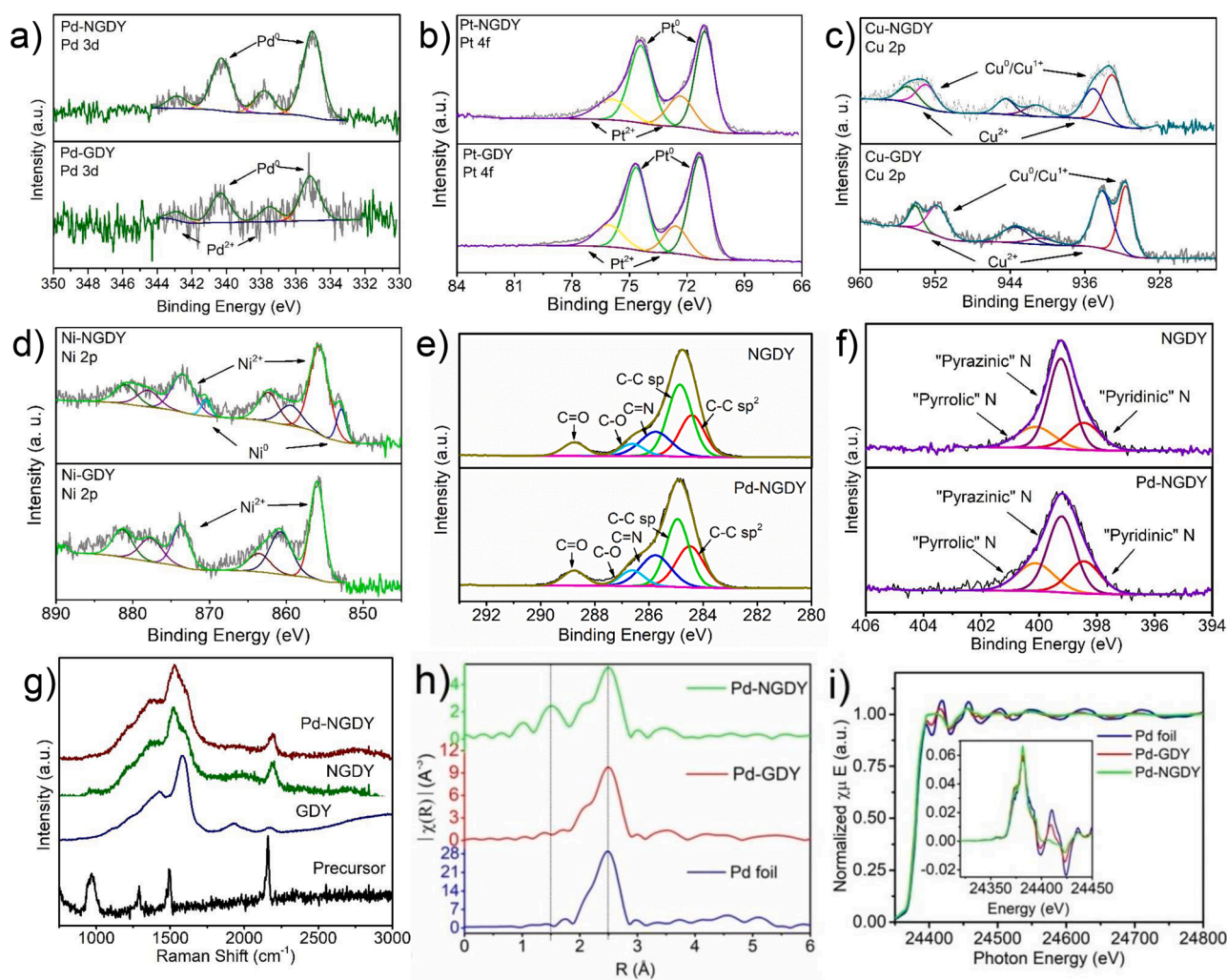The X-ray diffraction (XRD) diagram of Pd-NGDY was shown in Fig.

Fig. 3. High-resolution XPS spectra of a) Pd, b) Pt, c) Cu, d) Ni NPs on NGDY and GDY, respectively. High-resolution XPS spectra of e) C 1s and f) N 1s of NGDY before and after Pd deposition process. g) Raman spectra of precursors, GDY, NGDY, and Pd-NGDY. Pd K-edge EXAFS spectra h) and XANES profiles i) for Pd-NGDY, Pd-GDY, and Pd foil.

S4, in which the typical peak value (2 θ = 23°) of the two-dimensional material was clearly observed. However, no obvious palladium signal was observed because of its low loading and high dispersion. Raman spectra in Fig. 3g showed further characterization. Compared with the precursor, these two-dimensional materials showed widened peaks or bands. The Raman shifts of NGDY and GDY in D and G bands are different, but there is little difference in the vibration band of dialkynyl group, indicating that nitrogen doping in NGDY induced more electron changes and defects. Metal nanoparticles anchored hybrid materials, such as Pd-NGDY, showed typical D-band, G-band and dialkynyl vibration modes at 1349 cm^{-1}, 1540 cm^{-1}, and 2172 cm^{-1}. Pd NPs loading enhanced D/G ratio and slightly shifted D and G bands to lower wave number as compared with GDY and NGDY.

K-edge XANES profiles and Fourier transformed EXAFS spectra provide coordination information between metal NPs (taking Pd as an example) and substrate (Fig. 3h, I). Pd foil was set as the standard (EXAFS fitting parameters are showed in Table S6). Compared with Pd-GDY, the XANES profile of Pd-NGDY (Fig. 3h) was less similar to that of Pd foil, and more similar to that of Pd-N [51], which meant higher Pd^{2+}/Pd$^{\circ}$ ratio and less Pd atoms aggregation in Pd-NGDY (in line with XPS results), that is, N doping is beneficial to NPs dispersion. The Fourier transformed EXAFS spectra (Fig. 3i) provided Pd-Pd and Pd-N bonding details for Pd-NGDY and Pd-GDY. In Pd-NGDY, Pd-N and Pd-Pd bond distances were 0.203 and 0.275 nm, respectively, and the coordination numbers (CN) for Pd-N and Pd-Pd were 1.6 and 3.4, respectively. However, Pd-GDY showed a slightly shorter Pd-Pd bond distance (0.275 nm), and the coordination number was fitted as 6.6. At the same time, Pd-NGDY showed a different Pd-N peak profile at ~ 0.15 nm as compared with Pd-GDY and Pd foil, which also indicated the different coordination environment in Pd-NGDY, thus influence of the charge transfer between metal NPs and NGDY could be expected.

Brunauer-Emmet-Teller (BET) analysis was performed to determine the specific surface area of NGDY and Pd-NGDY. As shown in Fig. 4, N$_2$ adsorption and desorption isotherms indicated type IV curves for both NGDY and Pd-NGDY, and the BET surface area were 535 m^2 g^{-1} and 152 m^2 g^{-1}, respectively, which were at high level for carbon materials [37], implying high porosity of NGDY. Anchoring of Pd NPs on NGDY caused large decrease of N$_2$ adsorption of the material. The BET surface area of GDY was determined to be 666 m^2 g^{-1} (Fig. S5), a bit larger than NGDY.

3.2. Catalytic performance in the Suzuki-Miyaura reaction

Among all the prepared nanohybrid materials, Pd-NGDY was selected as the catalyst to investigate its activity in Suzuki-Miyaura reaction, and Pd-C was used as the control catalyst. Pd-GDY, an analogue with Pd NPs anchored on all carbon material GDY, was also involved in order to understand the role of substrate materials in catalysis. In order to obtain the best catalyst conditions, various solvents (Table S3), bases (Table S4) and temperatures (Table S5) were considered in the coupling reaction between bromobenzene and phenyl boric acid. Ethanol / water (7:4), K$_2$CO$_3$, and 80 °C were optimized as the best solvents, base and temperature for this reaction, without the need of phase transfer agents.

Only one biphenyl product was observed in all reactions. The lines chart in Fig. 5 comprehensively showed the catalytic activity of different catalysts, and the conversion rate changes with time (taking the coupling of iodobenzene and phenylboronic acid as the model reaction). The catalytic performance of Pd-NGDY is better than that of Pd-C and Pd-GDY. With the catalysis of Pd-NGDY, the conversion reached 75 % in 30 min, then over 90 % in 1 h, with the TOF number of 1287 h^{-1}, and the substrate/catalyst ratio was 497. In contrast, the coupling reaction efficiency of commercial Pd-C and Pd-GDY catalyst was relatively low. The conversion rate was only about 2/3 after 1 h, and the TOF value is about 700 h^{-1} for Pd-C. N-doping and chemical functional groups of supporting materials could promote the adsorption and activation for reactants [44], therefore Pd-NGDY showed superior catalytic performance than commercial Pd-C catalyst. At the same time, there were more borate coupling by-products at the end of the reaction catalyzed by Pd-GDY, which indicated that the N-doping of graphdiyne was beneficial to heterocoupling to a certain extent and inhibited homocoupling. Then, more than ten experiments of catalyst recovery were carried out. Fig. 5 also showed the progress of the 12th cycle of the coupling reaction, and Fig. S6 provided the high-resolution TEM image of Pd-NGDY after the 12th cycle. The catalytic activity of Pd NPs on NGDY was almost unchanged after 12th recycle, and there was no obvious aggregation of Pd NPs, indicating that Pd-NGDY was quite stable and recyclable.
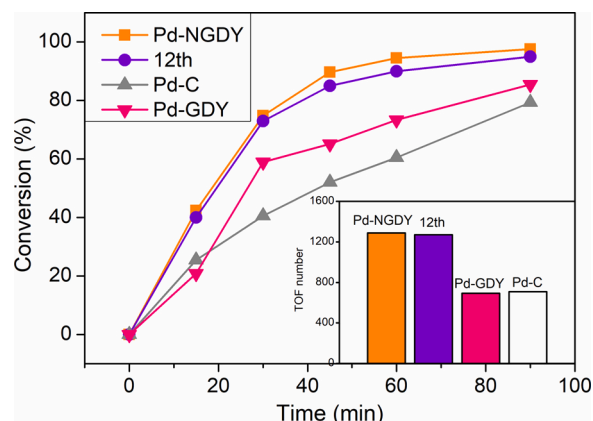
Fig. 5. Progress of Suzuki-Miyaura reactions under the catalyzing of different catalysts. Conditions: 0.5 mmol iodobenzene, 0.75 mmol phenylboronic acid, 1 mmol K$_2$CO$_3$, Ethanol/Water (7:4), 80 °C; 10 mg Pd-NGDY, reused Pd-NGDY, and Pd-C catalysts. Inset: TOF number of reactions using different catalysts.
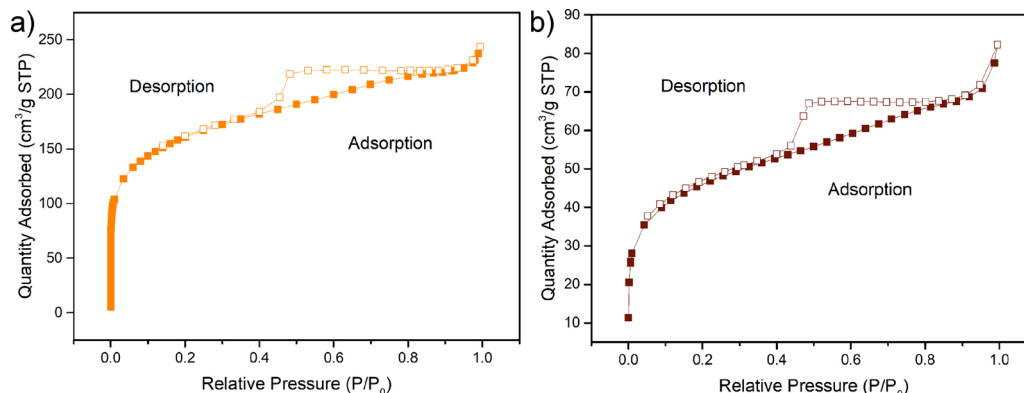
Fig. 4. N$_2$ adsorption and desorption isotherms of a) NGDY and b) Pd-NGDY.

Infrared spectroscopy (IR) study was carried out to understand the interactions between catalysts and reactants. Results were shown in Fig. S7 with IR spectra of dissociative reactant and adsorbed reactant on different Pd catalysts. *p*-Bromo benzaldehyde was employed as the reactant, and the vibration of aldehyde group served as the featuring signal. In general, 10 mg Pd catalyst was mixed with 100 μL ethanol containing 10 mg *p*-bromo benzaldehyde. Solvent volatilized at room temperature overnight before IR measurement. Compared with dissociative *p*-bromo benzaldehyde (1690 cm^{-1}), adsorbed reactant shifted the vibration wave number to 1692 cm^{-1}, 1695 cm^{-1}, 1697 cm^{-1}, 1698 cm^{-1}, and 1699 cm^{-1} in GDY, Pd-NGDY, NGDY, Pd-C, Pd-GDY, respectively. The spectroscopic shifts indicate the electron density variation of the adsorbed reactants, suggesting that Pd catalysts interact with reactants via charge transfer process. The IR vibration shift of reactant adsorbed on NGDY is much larger than that on GDY, which means stronger adsorption of reactant on NGDY. However, the smallest shift was observed for Pd-NGDY in the Pd series, which was related to the easier evolution for organic molecules and higher catalytic activity than other catalysts [23]. Although Pd-C was inferior to other Pd hybrids in catalytic performance, the IR vibration wave number of reactant adsorbed on it shifted more than that on Pd-NGDY, yet less than that on Pd-GDY, from which could be inferred that the activity of catalysts was determined not only by adsorption factor. In other words, N-doping resulted in electron density variation of NGDY and GDY, and further influenced the absorption of reactant, the Pd NPs binding, eventually the catalyst activity.
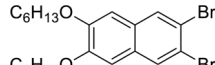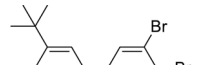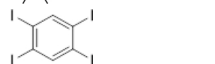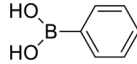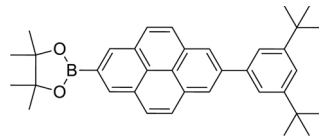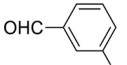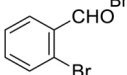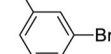
To evaluate the universality of Pd-NGDY catalyst, aryl halides containing donor or acceptor groups at different positions were investigated in Suzuki-Miyaura coupling reaction under the optimized reaction conditions. A series of coupling reactions catalyzed by Pd-NGDY are listed in Table 1. In all cases, except for the coupling reaction with chlorobenzene (entry 3, due to the weak reactivity of C-Cl), the coupling reaction catalyzed by Pd-NGDY shows extraordinary catalytic performance. The effects of electronic and steric effects on the yields and reaction rates were also studied. Compared with the electron donating substitutes, the electron withdrawing groups accelerated Suzuki-Miyaura reaction. The conversion rate of para-formyl substituted bromobenzene is the highest compared with *ortho* and *meta* substituted configurations (entry 4–7). A wide range of reactants, including 2-bromonaphthalene and 1,3-dibromobenzene, showed high yields (entry 8,9). Furthermore, the coupling reactions of conjugated groups substituted aryl halides and boronic compounds (entry 10–12) were also well catalyzed. Small molecule samples were analyzed by GC—MS, and large molecule product samples were characterized by NMR (Supplementary information). Various catalysts for Suzuki-Miyaura reaction in

Table 2

Comparison of catalysts for Suzuki-Miyaura reactions (bromobenzene and phenylboronic acid as reactants) in literature.

Catalyst	Solvent	Base	Temp	Time	Yield
NHC-Pd@GO [37]	EtOH-H$_2$O (1:1)	K$_2$CO$_3$	R. T	1 h	96 %
Pd/(RGO-PPD) [52]	EtOH-H$_2$O (1:1)	K$_2$CO$_3$	R. T	0.5 h	100 %
IL-RGO/Pd$_{2.5}$Cu$_{2.5}$ [45]	EtOH-H$_2$O (4:1)	K$_2$CO$_3$	80 ℃	1 h	94 %
Fe$_3$O$_4$@Boehmite-NH$_2$-Co$^{\parallel}$ [53]	H$_2$O	KOH	80 ℃	35 min	95 %
Pd-PVA [32]	EtOH	K$_2$CO$_3$	80 ℃	2.5 h	100 %
Pd-NGDY (this work)	EtOH-H$_2$O (7:4)	K$_2$CO$_3$	80 ℃	1.5 h	97 %
Pd-GDY (this work)	EtOH-H$_2$O (7:4)	K$_2$CO$_3$	80 ℃	3 h	95 %

Table 1

Substrate scope and yield of Pd-NGDY catalyzed Suzuki-Miyaura reaction.

Entry	Boronic acid		Entry	Boronic ester	
	Substrate	Yield (%)		Substrate	Yield (%)
1		99	**10a**		70
2		97	**11a**		67
3		trace	**12a**		80
4		95			
5		97	Boronic acid		
6		96			
7		94			
8		97	Boronic ester		
9		90			

Reaction conditions: 0.5mmol aryl halides, 1.5 equivalent boronic agent and 2 equivalent K$_2$CO$_3$ using Pd-NGDY catalyst in 11 ml EtOH-H$_2$O (v/v = 7:4), 80 ℃, 2 h. [a] Reaction conditions: toluene/ethanol = 3:1, 5 h.

literature were collected and compared in Table 2, from which we can see that the Pd-NGDY exhibited comparable performance with other reported catalysts considering the active Pd content.

The heterogeneity of Suzuki reactions catalyzed by Pd-NGDY was verified by hot filtration test. Under the optimum conditions, Pd-NGDY was used to catalyze the coupling reaction of bromobenzene and phenylboronic acid. During the half time of the reaction, Pd-NGDY catalyst was separated from the reaction mixture by rapid hot filtration to prevent the re-deposition of leached Pd species (if any), and the filtrate was reheated to the specified temperature to continue the reaction. GC—MS was used to monitor the reaction process. The results showed that after the removal of Pd-NGDY catalyst, the content of bromobenzene did not decrease, indicating that the real active catalyst is Pd nanoparticles on the surface of NGDY, rather than Pd species leached from Pd-NGDY. Namely, the reaction rate did not correlate with Pd amount in solution. In addition, TEM image of cycled Pd-NGDY catalyst showed negligible change in size and amount for Pd NPs (Fig. S6). The heterogeneous properties of Suzuki reactions catalyzed by Pd NPs have also been shown in literature [54].

3.3. DFT calculations

Composite catalysts with metal species anchored on GDY based materials have been used in various catalytic processes. Previous theoretical study reveals the structure of metal atoms located in the triangular corner of the pore of GDY [32]. Similar structure of Pd-NGDY is used as the model for DFT calculation in this work, and iodobenzene is used as the reaction substrate. As reported previously [55], the metal NPs anchored on graphene with abundant defect sites showed enhanced

charge transfer ability through lower the activation energy for different steps in Suzuki reaction. [23]. Considering the difficulty to precisely determine the atom number in each nanoparticle, tetrahedral clusters containing four Pd atoms, with high stability [23] and lower calculation workload, were used as an ideal model instead of nanoparticles in order to facilitate the calculation. Further calculations for more abundant information will be carried out in future efforts.

Geometry optimization (both atomic coordinates and cell parameters) and band structure calculations of NGDY were carried out using the VASP package with the PBE exchange-correlation functional within a generalized gradient approximation and the projector augmented-wave potential. The band gap of NGDY was calculated to be 0.50 eV. The high symmetric points locate at $\Gamma = (0, 0, 0)$, $S = (0, 1/2, 0)$, $Y = (-1/2, 1/2, 0)$, and the DOS of NGDY is zero at Fermi level (Fig. 6a). The electron distribution of Pd-NGDY is calculated and the charge transfer between Pd and NGDY is studied. Fig. 6b shows the red and green blocks that represent the electron poor and rich regions, respectively. It can be seen that the red block is mainly concentrated on the Pd nanoparticles anchored on the substrate, while the green block is mainly concentrated on the carbon and nitrogen atoms in NGDY, which means the charge transfer from NGDY to Pd nanoparticles, which is consistent with the experimental results [56]. The effective charge transfer (donation and acceptation) between metal species and supporting materials is beneficial for catalytic activity [55].

The free energy profile of Suzuki-Miyaura coupling reaction of iodobenzene catalyzed by Pd-NGDY is shown in Fig. 6c. Pd clusters absorbed on NGDY surface (E1) was set as zero. Iodobenzene molecules adsorbed on the surfaces of NGDY and Pd NPs to form state E2, and then C–I bond broke (E2 to E3). With the departure of halide group (E3),
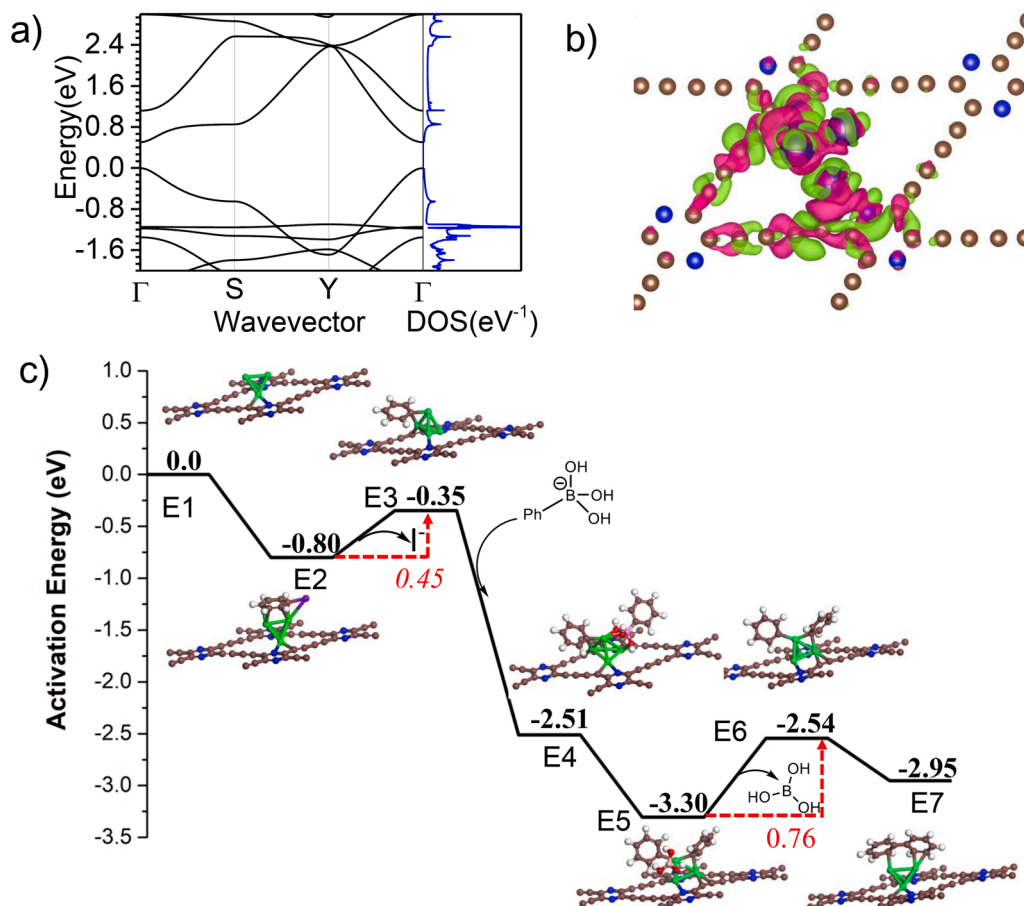

Fig. 6. a) Calculated band structure and density of states of NGDY. b) Charge difference density of Pd-NGDY. Red and green represent charge depletion and accumulation respectively. c) Free energy profile of the Pd-NGDY catalyzed Suzuki-Miyaura coupling reaction of iodobenzene and phenylboronic acid.

phenyl borate substituted halogen to form E4 state. The phenyl on borate migrated to Pd cluster (E5) and reached the transmetalation state (E6). Finally, before desorption, elimination produced the final product. The results showed that the energy of E2-E3 and E5-E6 keep upward, while the free energy tends to decrease, which is conducive to the coupling reaction. The reductive elimination process (from E5 to E7) needed to overcome an energy barrier of 0.76 eV that was bigger than the oxidative-addition step (E2 to E3, 0.45 eV), so it was considered as the rate-determining step. This was different from the classical cross-coupling reactions (between aryl halides and aryl boronic acids) that governed by the oxidative-addition step involved the halide-C bond breaking [57–59], which would resulted from the strong charge transfer from the substrates to Pd clusters [55]. In view of distinctive chemical and electronic structure, NGDY acted as a binding material for Pd NPs as well as electron reservoir to effectively reduce the activation energy of cross-coupling reaction.

4. Conclusions

In summary, we proposed a method to synthesize N-doped graphdiyne (NGDY) from tetraethynylpyrazine from bottom to top, which can generate specific pyridine nitrogen atoms in N-doped carbon materials. Considering N-doping and abundant alkynyl groups, this unique structure is a promising material for anchoring ultrafine metal nanoparticles (NPs) or clusters such as Pd, Pt, Cu, Ni. The natural pore structure will further help the binding of metal nanoparticles without purposeful producing of vacancy defect sites in commercial carbon materials. The introduction of nitrogen into the graphdiyne framework makes the metal NPs disperse without aggregation, and enhances the charge transfer between NGDY and metal nanoparticles. As an effective heterogeneous catalyst, Pd-NGDY complex has been applied in Suzuki-Miyaura reaction with high performance, with the TOF value as high as 1287 h^{-1}, which was better than commercial Pd-C catalyst. Our research showed that heteroatom doping was an effective way to adjust the electronic density of loaded metal nanoparticles through charge transfer, which had potential application in heterogeneous catalysis. More attention will be supposed to focus on metal-support complex modulating as well as catalytic mechanism in further work.

CRediT authorship contribution statement

Han Shen: Methodology, Investigation, Writing- Original draft preparation. **Jingyi He:** Data curation. **Feng He:** Calculation, Validation. **Yurui Xue:** Investigation. **Yongjun Li:** Conceptualization, Writing-Reviewing and Editing. **Yuliang Li:** Supervision.

Declaration of Competing Interest

The authors report no declarations of interest.

Acknowledgements

Appendix A. Supplementary data

Supplementary material related to this article can be found, in the online version, at doi:https://doi.org/10.1016/j.apcata.2021.118244.

References

[1] G. Li, Y. Li, H. Liu, Y. Guo, Y. Li, D. Zhu, Chem. Commun. 46 (2010) 3256–3258.
[2] Y. Li, L. Xu, H. Liu, Y. Li, Chem. Soc. Rev. 43 (2014) 2572–2586.
[3] Z. Jia, Y. Li, Z. Zuo, H. Liu, C. Huang, Y. Li, Acc. Chem. Res. 50 (2017) 2470–2478.
[4] C. Huang, Y. Li, N. Wang, Y. Xue, Z. Zuo, H. Liu, Y. Li, Chem. Rev. 118 (2018) 7744–7803.
[5] X. Gao, H. Liu, D. Wang, J. Zhang, Chem. Soc. Rev. 48 (2019) 908–936.
[6] Z. Zuo, D. Wang, J. Zhang, F. Lu, Y. Li, Adv. Mater. 31 (2019), 1803762.
[7] Y. Xue, B. Huang, Y. Yi, Y. Guo, Z. Zuo, Y. Li, Z. Jia, H. Liu, Y. Li, Nat. Commun. 9 (2018) 1460.
[8] J. Li, Y. Chen, J. Guo, F. Wang, H. Liu, Y. Li, Adv. Funct. Mater. 30 (2020), 2004115.
[9] J. He, N. Wang, Z. Cui, N. Du, L. Fu, C. Huang, Z. Yang, X. Shen, Y. Yi, Z. Tu, Y. Li, Nat. Commun. 8 (2017) 1172.
[10] Y. Zhao, J. Wan, H. Yao, L. Zhang, K. Lin, L. Wang, N. Yang, D. Liu, L. Song, J. Zhu, L. Gu, L. Liu, H. Zhao, Y. Li, D. Wang, Nat. Chem. 10 (2018) 924–931.
[11] R. Liu, H. Liu, Y. Li, Y. Yi, X. Shang, S. Zhang, X. Yu, S. Zhang, H. Cao, G. Zhang, Nanoscale 6 (2014) 11336–11343.
[12] H. Yu, Y. Xue, L. Hui, C. Zhang, Y. Zhao, Z. Li, Y. Li, Adv. Funct. Mater. 28 (2018), 1707564.
[13] Y. Zhao, N. Yang, H. Yao, D. Liu, L. Song, J. Zhu, S. Li, L. Gu, K. Lin, D. Wang, J. Am. Chem. Soc. 141 (2019) 7240–7244.
[14] H. Shang, Z. Zuo, H. Zheng, K. Li, Z. Tu, Y. Yi, H. Liu, Y. Li, Y. Li, Nano Energy 44 (2018) 144–154.
[15] X. Kan, Y. Ban, C. Wu, Q. Pan, H. Liu, J. Song, Z. Zuo, Z. Li, Y. Zhao, ACS Appl. Mater. Interfaces 10 (2018) 53–58.
[16] Q. Pan, H. Liu, Y. Zhao, S. Chen, B. Xue, X. Kan, X. Huang, J. Liu, Z. Li, ACS Appl. Mater. Interfaces 11 (2019) 2740–2744.
[17] X. Zhu, Y. Zhu, S. Murali, M.D. Stoller, R.S. Ruoff, ACS Nano 5 (2011) 3333–3338.
[18] S.E. Gilliland III, J.M.M. Tengco, Y. Yang, J.R. Regalbuto, C.E. Castano, B. F. Gupton, Appl. Catal. A-Gen. 550 (2018) 168–175.
[19] S. Guo, D. Wen, Y. Zhai, S. Dong, E. Wang, ACS Nano 4 (2010) 3959–3968.
[20] S. Moussa, A.R. Siamaki, B.F. Gupton, M.S. El-Shall, ACS Catal. 2 (2012) 145–154.
[21] A.R. Siamaki, A.E.R.S. Khder, V. Abdelsayed, M.S. El-Shall, B.F. Gupton, J. Catal. 279 (2011) 1–11.
[22] R. Kumar, J.-H. Oh, H.-J. Kim, J.-H. Jung, C.-H. Jung, W.G. Hong, H.-J. Kim, J.-Y. Park, I.-K. Oh, ACS Nano 9 (2015) 7343–7351.
[23] Y. Yang, C.E. Castano, B.F. Gupton, A.C. Reber, S.N. Khanna, Nanoscale 8 (2016) 19564–19572.
[24] I.C. Gerber, P. Serp, Chem. Rev. 120 (2020) 1250–1349.
[25] Y. Yang, A.C. Reber, S.E. Gilliland III, C.E. Castano, B.F. Gupton, S.N. Khanna, J. Catal. 360 (2018) 20–26.
[26] M. Zhao, Y. Wu, J.-P. Cao, Appl. Organomet. Chem. 34 (2020).
[27] R.L. Oliveira, J. Kerstien, R. Schomaecker, A. Thomas, Catal. Sci. Technol. 10 (2020) 1385–1394.
[28] L. Wang, S. Ma, Z. Jiao, D. Yuan, Appl. Surf. Sci. 465 (2019) 1–9.
[29] H. Shen, Y. Li, Z. Shi, ACS Appl. Mater. Interfaces 11 (2019) 2563–2570.
[30] H. Qi, P. Yu, Y. Wang, G. Han, H. Liu, Y. Yi, Y. Li, L. Mao, J. Am. Chem. Soc. 137 (2015) 5260–5263.
[31] I.P. Beletskaya, F. Alonso, V. Tyurin, Coord. Chem. Rev. 385 (2019) 137–173.
[32] E. Hariprasad, T.P. Radhakrishnan, ACS Catal. 2 (2012) 1179–1186.
[33] M. Keyhaniyan, A. Shiri, H. Eshghi, A. Khojastehnezhad, New J. Chem. 42 (2018) 19433–19441.
[34] X. Yan, Y. Luo, W. Liu, L. Liang, Y. Gan, Z. Chen, Z. Xu, D. Wan, H. Shi, J. Hu, Phys. Chem. Chem. Phys. 22 (2020) 6222–6230.
[35] J.A. Bobb, A.A. Ibrahim, M.S. El-Shall, ACS Appl. Nano Mater. 1 (2018) 4852–4862.
[36] Y. Yang, S.E. Gilliland III, S. Ghobadi, M. Burkholder, S.E. Smith, B.F. Gupton, C. E. Castano, React. Chem. Eng. 4 (2019) 90–99.
[37] V. Kandathil, B. Kulkarni, A. Siddiqa, M. Kempasiddaiah, B.S. Sasidhar, S.A. Patil, S.A. Patil, Catal. Lett. 150 (2020) 384–403.
[38] G. Kresse, J. Furthmüller, Comp. Mater. Sci. 6 (1996) 15–50.
[39] G. Kresse, J. Furthmüller, Phys. Rev. B 54 (1996) 11169.
[40] J.P. Perdew, K. Burke, M. Ernzerhof, Phys. Rev. Lett. 77 (1996) 3865–3868.
[41] H.J. Monkhorst, J.D. Pack, Phys. Rev. B 13 (1976) 5188–5192.
[42] J.K. Nørskov, J. Rossmeisl, A. Logadottir, L. Lindqvist, J.R. Kitchin, T. Bligaard, H. Jónsson, J. Phys. Chem. B 108 (2004) 17886–17892.
[43] A. Petrosyan, P. Ehlers, A.-E. Surkus, T.V. Ghochikyan, A.S. Saghyan, S. Lochbrunner, P. Langer, Org. Biomol. Chem. 14 (2016) 1442–1449.
[44] R. Nie, M. Miao, W. Du, J. Shi, Y. Liu, Z. Hou, Appl. Catal. B 180 (2016) 607–613.
[45] Y. Ru, Y. Huang, Y. Wang, L. Dai, Appl. Organomet. Chem. 33 (2019) e5198.
[46] M. Sahoo, S. Mansingh, S. Subudhi, P. Mohapatra, K. Parida, Catal. Sci. Technol. 9 (2019) 4678–4692.
[47] Y. Su, K. Fu, Y. Zheng, N. Ji, C. Song, D. Ma, X. Lu, R. Han, Q. Liu, Appl. Catal. B 288 (2021), 119980.
[48] W. Li, X.-s. Chu, F. Wang, Y.-y. Dang, X.-y. Liu, X.-c. Wang, C.-y. Wang, Appl. Catal. B 288 (2021), 120034.
[49] N. Cheng, Q. Liu, A.M. Asiri, W. Xing, X. Sun, J. Mater. Chem. A 3 (2015) 23207–23212.

[50] H. Yu, W. Tang, K. Li, H. Yin, S. Zhao, S. Zhou, Chem. Eng. Sci. 196 (2019) 402–413.

[51] Y. Ryou, J. Lee, S.J. Cho, H. Lee, C.H. Kim, D.H. Kim, Appl. Catal. B: Environ. 212 (2017) 140–149.

[52] A.A. Ibrahim, A. Lin, M.S. Adly, M.S. El-Shall, J. Catal. 385 (2020) 194–203.

[53] A. Mohammadinezhad, B. Akhlaghinia, Green Chem. 19 (2017) 5625–5641.

[54] M. Zhao, Y. Wu, Appl. Organomet. Chem. 34 (2020).

[55] Y. Yang, A.C. Reber, S.E. Gilliland, C.E. Castano, B.F. Gupton, S.N. Khanna, J. Phys. Chem. C 122 (2018) 25396–25403.

[56] Q.-Q. Yan, D.-X. Wu, S.-Q. Chu, Z.-Q. Chen, Y. Lin, M.-X. Chen, J. Zhang, X.-J. Wu, H.-W. Liang, Nat. Commun. 10 (2019) 4977.

[57] C.A. Fleckenstein, H. Plenio, Chem. Soc. Rev. 39 (2010) 694–711.

[58] J.F. Hartwig, Nature 455 (2008) 314–322.

[59] L. Xue, Z. Lin, Chem. Soc. Rev. 39 (2010) 1692–1705.